Matter and Radiation at Extremes | RESEARCH ARTICLE | scitation.org/journal/mre

Experimental study of residual activity induced in aluminum targets irradiated by high-energy heavy-ion beams: A comparison of experimental data and FLUKA simulations

Cite as: Matter Radiat. Extremes 4, 055403 (2019); doi: 10.1063/1.5097035
Submitted: 22 March 2019 • Accepted: 22 May 2019 •
Published Online: 5 September 2019

Peter Katrík,[1,a] Dieter H. H. Hoffmann,[2,3,a] Edil Mustafin,[1] and Ivan Strašík[1]

AFFILIATIONS

[1]GSI Helmholtzzentrum für Schwerionenforschung, Planckstrasse 1, 64291 Darmstadt, Germany
[2]School of Science, Xi'An Jiaotong University, Xianning West Road 28, Xi'An 7100049, China
[3]National Research Nuclear University MEPhI, Moscow, Russia

[a]**Authors to whom correspondence should be addressed:** p.katrik@gsi.de and Hoffmann@xjtu.edu.cn

ABSTRACT

A number of heavy-ion accelerators are either under construction (e.g., the Facility for Antiproton and Ion Research in Darmstadt and the High Intensity Accelerator Facility in China) or already in operation at many places worldwide. For these accelerators, activation of construction components due to beam loss, even during routine machine operation, is a serious issue, especially with the upcoming high-intensity facilities. Aluminum is one of the most commonly used construction materials in beam lines, collimators, and other components. Therefore, we report here on activation experiments on aluminum samples to verify and benchmark simulation codes. The analysis was performed by gamma spectroscopy of the irradiated targets. Our results on the induced activity measured in samples irradiated by uranium beams at 125 MeV/u and 200 MeV/u and a xenon beam at 300 MeV/u show activation levels significantly lower than those predicted by FLUKA simulations.

I. INTRODUCTION

The physics and technology of accelerators have undergone remarkable developments since their invention in the last century. Owing to the de Broglie relation $\lambda = h/p$ between particle momentum p, wavelength λ, and Planck's constant h, there has been a longstanding quest for higher energies to allow the structure of matter to be probed in greater detail at smaller scales. This development has currently culminated in the construction of the Large Hadron Collider (LHC) at the European Nuclear Research Centre (CERN).[1] Of course, there has also always been the need for high-intensity beams to ensure that sufficient statistics can be obtained within a reasonable experimental time. Accelerators have also now achieved a firm place in industrial applications and even medical treatment.[2] There are numerous areas of application on the horizon that are within the energy range of a few GeV, much below the TeV regime of the LHC, but with a much higher demand on beam intensity. The ultimate challenge for high-intensity accelerators arises from accelerator-driven inertial fusion energy.[3] In this scenario, intense beam pulses are required to deliver up to 10 MJ per pulse to drive a fusion target.[4,5] The advanced accelerator-driven nuclear energy systems or nuclear waste incinerators that are under discussion[6] require high-intensity beams. High beam intensities are also required for high-energy-density physics (HEDP) experiments and for the production of rare isotope beams, envisioned for the ambitious heavy-ion projects currently under construction.[7–10] These are the Facility for Antiproton and Ion Research (FAIR) at GSI Darmstadt, the High Intensity Accelerator Facility (HIAF) in China, and the Facility for Rare Isotope Production (FRIB) at Michigan State University. These facilities will serve a wide range of research projects, including nuclear structure studies, investigations of compressed hadronic matter, and laboratory nuclear astrophysics, as well as HEDP. The beam intensities of FAIR, HIAF, and FRIB will be up to a factor of 1000 higher than those presently available.

With such facilities in mind, therefore, we have studied heavy-ion beam-induced activation of aluminum, which is a commonly used construction material for components of accelerators. Activation of

accelerator components is a process that cannot be ignored, even during normal machine operation, where it can influence or even restrict "hands-on" maintenance. The final goal of the work described here was to specify a criterion for tolerable beam loss valid for heavy-ion machines after long-term operation. Moreover, we aimed to validate the reliability of the criterion and clarify its credibility based on experimental data as well as simulation results. Thus, validation of the physical models and data libraries implemented in the simulation codes was necessary. We performed several irradiation experiments under different conditions at GSI Helmholtzzentrum für Schwerionenforschung in Darmstadt,[11–18] where we created an inventory of induced radioactive nuclides and measured the depth profiles of their residual activities and the ranges of primary particles. To establish the depth profiles, we used gamma-spectroscopic measurements of aluminum foils assembled in three different targets. The targets were irradiated by either ^{238}U or ^{124}Xe ion beams. To estimate the range of the primary particles, the simulation codes FLUKA 2011,[19,20] SRIM-2013,[21] and ATIMA[22] were used. The target stack, consisting of many foils, was arranged in such a way that high spatial resolution of the depth profiles was obtained in the predicted range region. The accuracy of the stopping power implemented in the codes was thereby tested.

In our experiments, measurement of the range of the ^{238}U primary beam by gamma spectroscopy was not possible owing to the very long half-life $T_{1/2} = 4.4 \times 10^9$ years. However, the ^{237}U nuclide with a half-life of 6.75 days was a suitable candidate projectile fragment. The range of nuclides with identical initial energy per nucleon is approximately proportional to A/Z^2 (where A is the mass number and Z is the atomic number). Thus, the range of the ^{237}U fragments is very close to that of the ^{238}U primary ions, regardless of where the fragmentation occurred.[16,23] A similar situation cannot arise for the ^{124}Xe beam, because none of the lighter fragments of the xenon ions are present in a statistically significant amount in our measured gamma spectra.

II. EXPERIMENTS AND METHOD

Three aluminum targets designated T_1, T_2, and T_3 were individually irradiated by different heavy-ion beams at a beam-dump experimental station of the SIS-18 heavy-ion synchrotron at GSI Darmstadt. The targets were made of 99.95% natural aluminum with a density of 2.70 g/cm^3 at 20 °C and consisted of a stack of foils (as shown in Fig. 1) to enable measurement of residual activity as a function of target depth.

The subdivision of the target into a stack of individual foils made it possible to determine the induced activity as a function of target depth by measuring the gamma spectrum of each foil. We assembled the foils (disk-shaped) into a so-called stacked-foil geometry (see Fig. 1). The total thickness of the target as well as the number of foils per target stack varied according to the expected range of the primary particles in the bulk of the target material. The targets were designed to locate the range region approximately in the middle of the target body. Since the highest depth resolution is necessary at the end of the particle track, the thinnest foils were ordered along the whole length of the target, with increasing number of foils in the middle. The thickness of the foils varied between 0.1 mm and 1.0 mm. In some cases, several foils were grouped together into one batch for activity measurement. These foils represented positions upstream and downstream of the range region, where high depth resolution was not necessary. Targets T_1 and T_2 were irradiated by ^{238}U beams with initial energies 200 MeV/u and 125 MeV/u, respectively. Target T_3 was irradiated by a ^{124}Xe beam with initial energy 300 MeV/u. The beam energies are not the on-target energies but the extraction energies measured at the SIS-18 accelerator. The fast-extraction regime of the machine was set with the beam pulses on target every 2–3 s ($\frac{1}{2}$–$\frac{1}{3}$ Hz). Information about the irradiation parameters is provided in Table I, where the irradiation time is the period between the first and last pulse including the beam-off periods.

The beam intensity of each experiment was determined using DC current transformers (DCCTs) measuring the beam current of each pulse intercepting these devices. A combination of DCCTs with other beam diagnostic instruments and software allows determination of the total number of ions with an uncertainty of about 3%.[24–27] Target foils were placed in aluminum holders mounted onto a movable platform at a distance of 60 cm from the vacuum window. This window was made of stainless steel with a thickness of 100 μm. The thickness of the vacuum window and the air gap were taken into account in the simulation model.

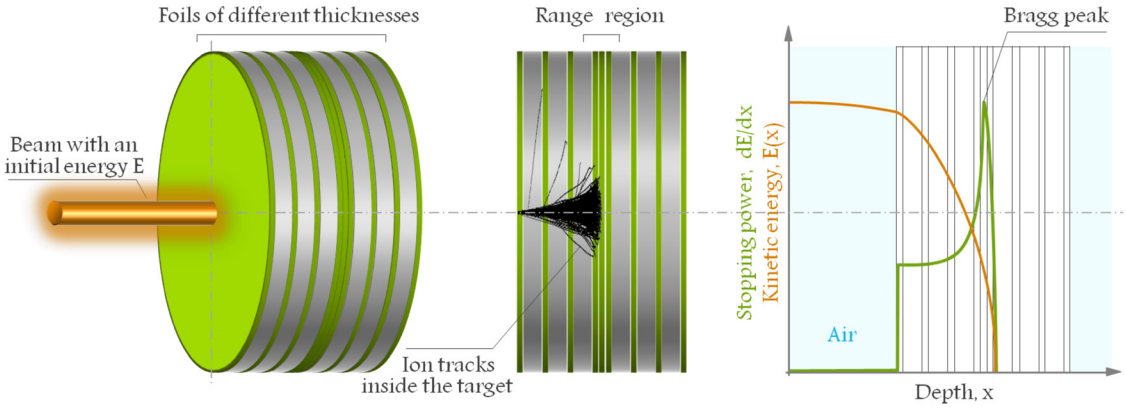

FIG. 1. Schematic representation of the targets used for the activation study. Separated disk-shaped foils with different thicknesses were used to achieve high resolution of the depth profiles and precise location of the range region. The diagram on the right shows the kinetic energy of the primary ions as a function of depth, as well as the maximum stopping power (Bragg peak) located in the range region. Note that the ion tracks shown in this figure correspond to a point-like primary beam calculated by SRIM.[21]

TABLE I. Parameters of aluminum targets and irradiation conditions.

Target	Beam	Beam charge state	Energy (MeV/u)	Total number of ions	Irradiation time (s)	Number of foils	Thickness of target (mm)	Diameter (mm)
T_1	^{238}U	+73	200	2.861×10^{12}	14 313	70	7.0	100.0
T_2	^{238}U	+89	125	1.183×10^{12}	8 037	16	1.6	100.0
T_3	^{124}Xe	+48	300	2.486×10^{12}	5 220	73	25.3	50.0

The acquisition of the gamma spectra started after the dose rates of the irradiated samples reached acceptable levels for safe transportation outside the radiation-controlled area, which is a dose rate below 6 mSv/year (this is an equivalent to 3 μSv/h) according to the radiation protection limits in force in Germany.[28] A typical gamma spectrum obtained from an aluminum sample after irradiation with a uranium-ion beam of 200 MeV/u is shown in Fig. 2. Collecting sufficient statistics on the gamma spectrum of each foil depended on its activation level, and this fluctuated between several hours and a few days. The foils of target T_1 were measured in two sets at different time-points of the decay: the first set within the range 6–22 days and the second set within the range 133–180 days after the end of irradiation. Target T_2 was measured in three sets: the first within 16–34 days, the second within 128–144 days, and the third within 260–285 days after the end of irradiation. Target T_3 was also measured in three sets: the first within 9–38 days, the second within 218–293 days, and the third within 378–505 days after the end of irradiation. Experimental data from each individual set of measurements are also labeled, with Figs. 4–9 showing depth profiles of different nuclides. A high-purity germanium (HPGe) detector manufactured by the Canberra Company, with an energy resolution of 1.8 keV FWHM at the 1332 keV ^{60}Co line, was used for recording all gamma spectra. The partial activity of each isotope was obtained from the peak-net-area (PNA) determined by GammaVision software, including the uncertainty in PNA.

III. COMPUTER SIMULATIONS

The experiments presented in this work were supported by several preliminary calculations in order to achieve the most precise prediction of the range region of the primary particles. Three different codes were used: FLUKA 2011,[20] SRIM-2013,[21] and ATIMA.[22] The SRIM and ATIMA codes are less complex and require shorter computation time. Therefore, they are frequently chosen for calculations of physical quantities related to the interaction of ions with matter, such as stopping power, energy loss, range, and angular straggling. Figure 3 shows the energy deposition distribution in the bulk of the target material calculated by FLUKA. Nuclear reactions cause fragmentation of primary ions and target atoms, which leads to smearing out of the Bragg-peak region of the energy deposition.

Results from SRIM and ATIMA were applied to quantification of the range and of range straggling. It should be clarified here, for correct interpretation of the presented data, that ATIMA and SRIM do not provide for inelastic interactions (nor does the TRIM Monte Carlo module of SRIM). Thus, fragmentation of the primary particles along their penetration path in the target is not simulated. More precise results are available from simulations performed with FLUKA (see Fig. 3). This is a multipurpose Monte Carlo software package containing a broad spectrum of possible settings of beam properties such as energy, beam size, and momentum spread of the incident beam. It is also possible to choose different physics models. Another advantage is that FLUKA allows the introduction of momentum spread of the incident beam. FLUKA has a collection of hadron–hadron (H-H), hadron–nucleus (H-N), and nucleus–nucleus (N-N) interaction models, among which, by default, it makes an autonomous choice, depending on the type and energy of the colliding objects. However, if necessary, users have the option to set the threshold energy of the model exchange. This option was essential for testing the transition between the relativistic quantum molecular dynamics (RQMD) and Boltzmann master equation (BME) models. Both of these are N-N interaction models covering the range of beam

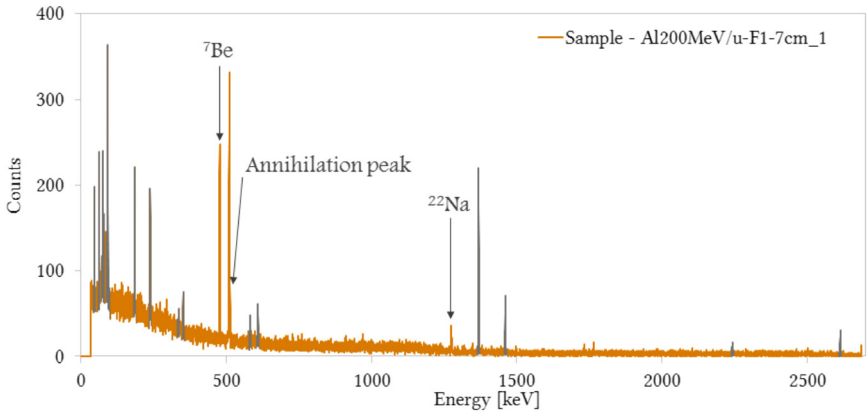

FIG. 2. Typical spectrum obtained from aluminum foil No. 1 located 3.2 mm upstream of the range of ^{238}U ions with energy 200 MeV/u (depth in the target = 0.25 mm). Gamma peaks of the background are shown in gray.

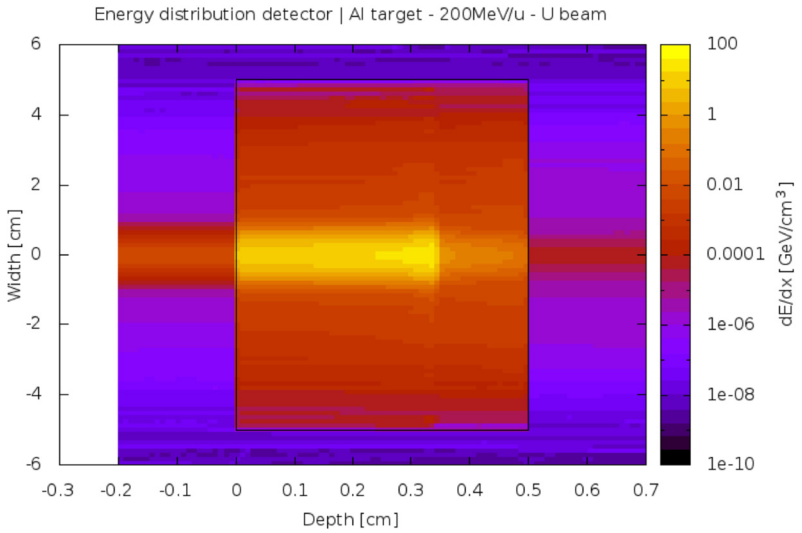

FIG. 3. Example of the stopping power distribution in the horizontal plane calculated with FLUKA for the case of ^{238}U ions with nominal energy 200 MeV/u after penetrating through the air gap and the aluminum target.

energies used in our study. The RQMD model is designed for simulating the appropriate conditions and behavior of nuclei participating in interactions within the range of energies from 0.125 GeV/u to 5 GeV/u, according to the user's manual for the FLUKA code.[19] The BME model is available in FLUKA 2011 and constitutes an important update of FLUKA 2008, since the new code version is capable of simulating N-N interactions below 0.125 GeV/u. Switching between these models takes place at a projectile energy of 0.125 GeV/u. In reality, this is not a strictly defined value, and there is a threshold range of ±0.025 GeV/u, which is also editable by FLUKA users. This means that FLUKA with the default setting of N-N interaction models uses both of them from 0.100 GeV/u to 0.150 GeV/u.[19] In brief, in the present study, heavy-ion transportation with nuclear interactions was switched on, electromagnetic dissociation was activated for all heavy-ion beams as well as for target nuclei, emission of high-energy light fragments through the coalescence mechanism was applied, and, finally, a new evaporation model with heavy-fragment evaporation was used and set in the input files for the FLUKA calculations.

IV. COMPARISON OF THE RESULTS

Nuclides produced during irradiation or during decay processes were identified, and their total residual activities induced in the targets were quantified and extrapolated to the end of irradiation and normalized per incident ion. The benchmarking also considered the shape of the depth profiles as a possible source of information about the fragmentation process of the primary particles and the target nuclei. The target-nuclei fragments can be observed from the first foil and extend beyond the range of the primary particles. The depth profiles of the projectile fragments start at the end of range of the primary ions. This corresponds to fragmentation of the primary particles at the very end of their penetration path. The fragments are

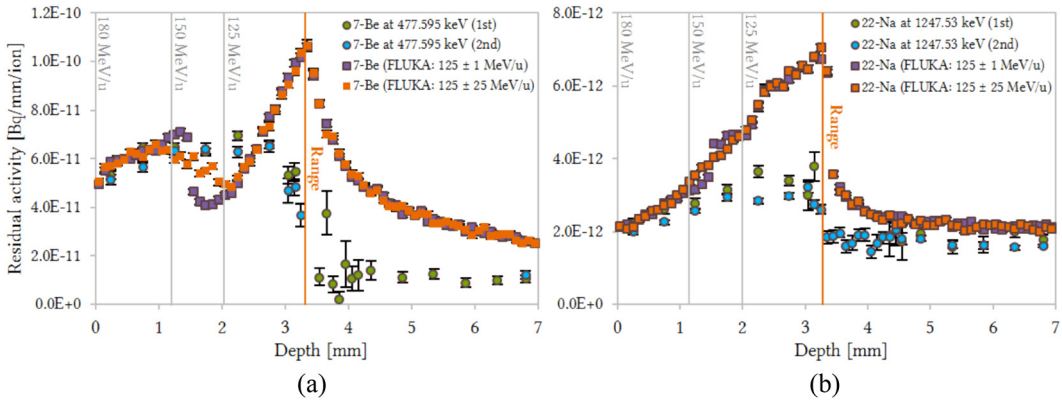

FIG. 4. Depth profiles of the residual activity of ^{7}Be (a) and ^{22}Na (b) in the aluminum target T_1 irradiated by ^{238}U with energy 200 MeV/u and two different FLUKA settings (BME-RQMD energy-threshold).

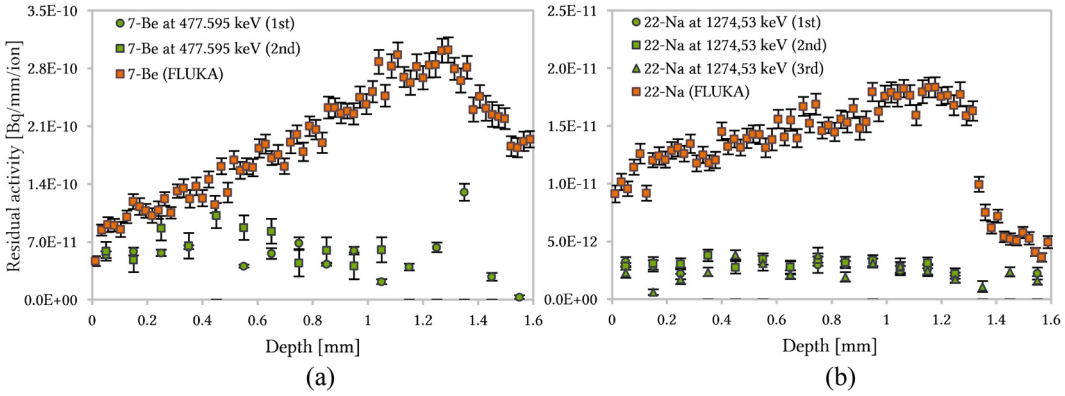

FIG. 5. Depth profiles of the residual activity of ^{7}Be (a) and ^{22}Na (b) in the aluminum target T_2 irradiated by ^{238}U with energy 125 MeV/u.

detectable in the foils downstream beyond the maximum range of the primary beam particles. Fragmentation of the primary ions at the beginning of their tracks leads to creation of lower-Z fragments with longer range.[16,18] Examples of the depth profiles of the ^{7}Be and ^{22}Na nuclides as typical target-nuclei fragments of the irradiation experiments on the aluminum targets T_1–T_3 are shown in Figs. 4–6.

Figure 4 presents the depth profiles obtained from irradiation of the T_1 target by a 200 MeV/u ^{238}U beam, which was described in detail with more examples in Ref. 18. Examination of these depth profiles uncovered a significant discrepancy between experimental data and simulation results. This is clearly visible in Fig. 4. Another important observation is that the disparity of the FLUKA calculations with experiment is correlated with the energy of the primary projectiles. The vertical lines in Fig. 4 represent the depths at which primary particles are slowed down to the respective energy indicated at these lines. Especially in the case of ^{7}Be, it is remarkable that in the energy range between 150 MeV/u and 125 MeV/u, FLUKA shows an oscillatory behavior, which is not seen in the experimental data. FLUKA switches between the RQMD and the BME interaction models at an energy of 125 MeV/u, with the default setting of the energy threshold at 125 ± 25 MeV/u.[19] This motivated us to study the influence of different settings for the RQMD-BME transition. Results for energy thresholds of 125 ± 25 MeV/u (FLUKA default) and 125 ± 1 MeV/u (our settings) are displayed in Fig. 4. Indeed, a change in the depth profiles between these different FLUKA settings (shown in orange and purple) is visible. However, none of the chosen settings improved the mismatch between experimental and calculated data. Moreover, the threshold settings of 125 ± 1 MeV/u reveal even larger deviations of the induced activity deep within the target, where the experimental data do not have any local extrema.

Similarly, the depth profiles shown in Figs. 5 and 6 demonstrate the overestimation of the residual activity by FLUKA, as well as the prediction of a peak-like depth-profile shape. It should be clarified that target T_2 was previously planned to be irradiated by a uranium beam with energy 100 MeV/u, but technical difficulties did not allow us to use energies below 125 MeV/u. Therefore, the range region of the primary particles is not in the center of the target, and the shape of the depth profile downstream of the range is not available. Nevertheless, part of the depth profile upstream of the range region is accessible for data analysis, and the measurement error is found to be smaller than the difference between experiment and simulation.

A depth-profile analysis of the residual activity of radionuclides induced in the T_3 target irradiated by 300 MeV/u ^{124}Xe beam revealed an unusual deviation of the measured data from the simulated results. For instance, in the case of ^{46}Sc, ^{48}V, ^{52}Mn, ^{54}Mn, ^{56}Co, ^{58}Co, and ^{65}Zn nuclides, FLUKA predicts an artificial increase in their residual

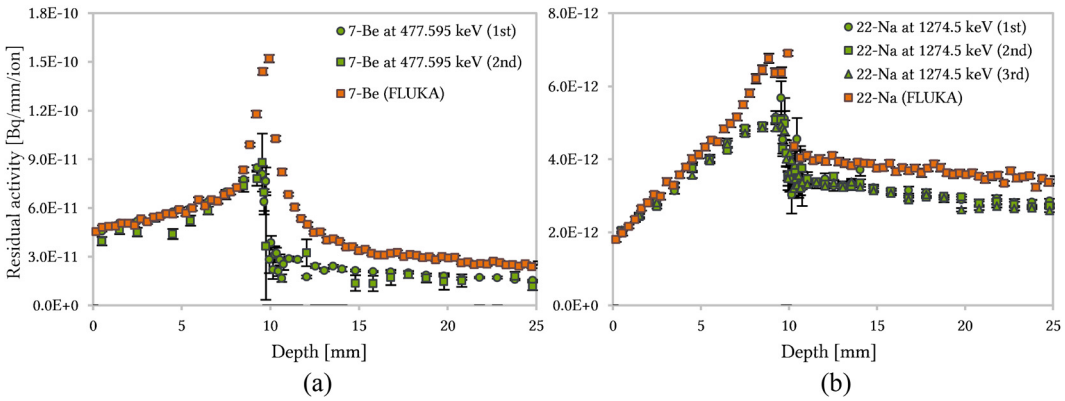

FIG. 6. Depth profiles of the residual activity of ^{7}Be (a) and ^{22}Na (b) in the aluminum target T_3 irradiated by ^{124}Xe with energy 300 MeV/u.

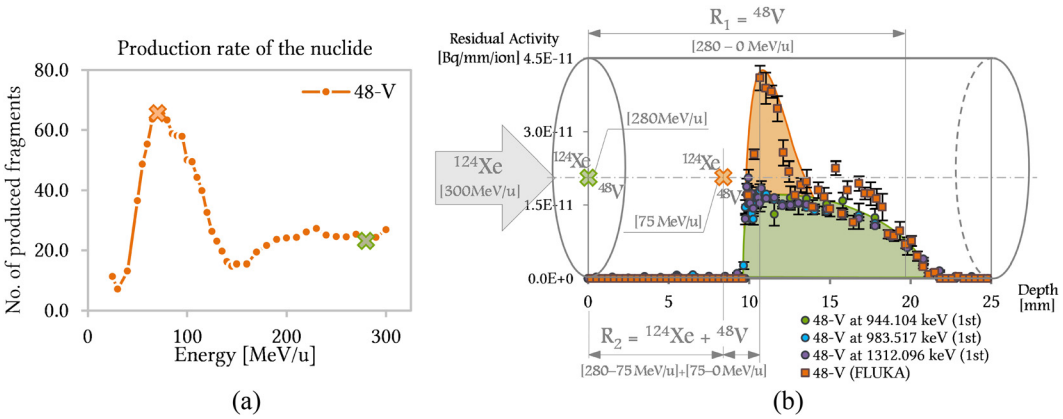

FIG. 7. Depth profile of residual activity of ^{48}V in an aluminum target irradiated by ^{124}Xe with energy 300 MeV/u (b) and the production rate of the nuclide in thin foil (a).

activity in a small region downstream of the range of the primary particles, while the experimental data do not support this. Therefore, we decided to study the production rate of these intermediate-Z fragments produced by ^{124}Xe passing through an aluminum foil. The production rate was scored as the number of fragments exiting the aluminum foil via its back surface. A study was performed as a set of several simulations of different xenon beams with energies between 25 MeV/u and 300 MeV/u penetrating through the different-thickness aluminum foils. To ensure identical conditions for all investigated beam energies, the thickness of each foil was set in such a way that the primary xenon ions lost 10% of their kinetic energy in the foil. With the set of simulations prepared in this way, we expected to find homogenous production rates without any local extrema that depended on the kinetic energy of the primary particles. However, it was observed that the production rate of intermediate-Z fragments was uniform only in the range of energies of xenon ions between 150 MeV/u and 300 MeV/u, but the production rate of the fragments was higher by a factor of about 3, as the kinetic energy of primary particles decreased to about 80 MeV/u according to the FLUKA simulations (as examples, the ^{48}V, ^{54}Mn, and ^{58}Co production rates are shown in Figs. 7–9). These results violate the expectation of a homogenous production rate, and they may be considered as an explanation of an artificially high residual activity predicted by FLUKA compared with the experimentally measured residual activities of the intermediate-Z fragments. In the following, we will explain how this inaccuracy of the FLUKA code influences the shapes of the depth profiles. The depth profile of the ^{48}V fragment shown in Fig. 7 will serve this purpose, but the same approach may be applied to all mentioned intermediate-Z fragments. In Fig. 7, the depth profile of the residual activity of ^{48}V is divided into two parts: the green area represents the correct, experimentally measured activity, and the orange area represents the incorrect, simulated activity. The green area corresponds to the residual activity of ^{48}V fragments, as if their production rate were homogenous regardless of the kinetic energy of the primary xenon ions. Every ^{48}V fragment is created by collision of a primary xenon ion and an aluminum atom of the target, where the kinetic energy of the newly created fragment is similar to the kinetic energy of the xenon ion shortly before collision. This fragment may penetrate through the target until it loses all its kinetic energy, or it may be fragmented into even lighter fragments.[14,16,18] The greater the depth at which the xenon ion collides and creates a ^{48}V ion, the less kinetic energy is transferred to the ^{48}V fragment, and this also determines the range of the fragment and where it will contribute to residual activity in the depth profile. Thus, the depth of penetration of a fragment is always the sum of the length of the primary-ion path to the place where that fragment was created and the range of the fragment itself. In Fig. 7, there are two examples, marked by a green cross (where the kinetic energy of

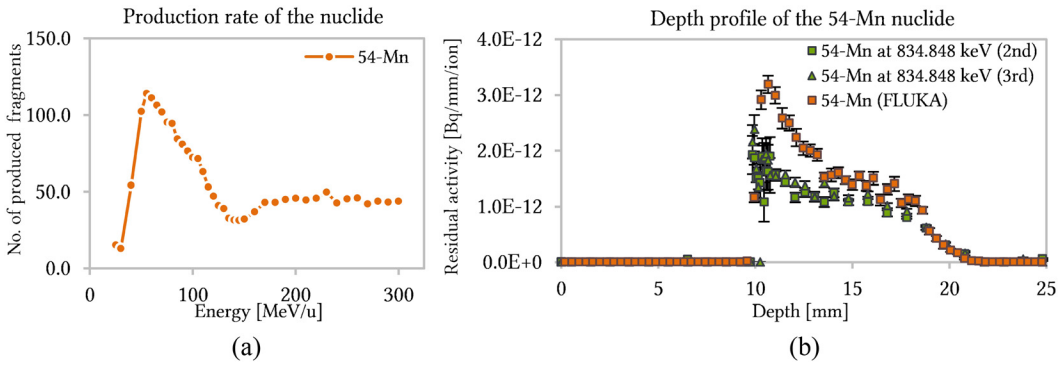

FIG. 8. Depth profile of residual activity of ^{54}Mn in an aluminum target irradiated by ^{124}Xe with energy 300 MeV/u (b) and the production rate of the nuclide in thin foil (a).

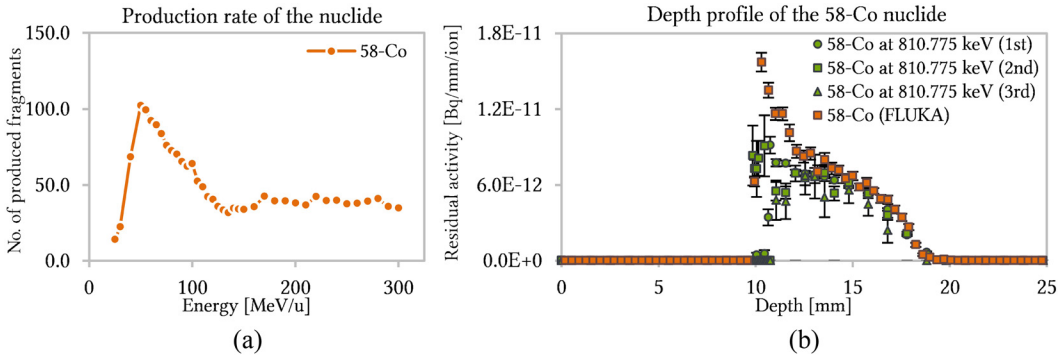

FIG. 9. Depth profile of residual activity of ^{58}Co in an aluminum target irradiated by ^{124}Xe with energy 300 MeV/u (b) and the production rate of the nuclide in thin foil (a).

TABLE II. Comparison of calculated and measured ranges of ^{238}U and ^{237}U induced in an aluminum target irradiated by ^{238}U ions with energy 200 MeV/u.

	Range ± range straggling (mm)			
Nuclide	ATIMA	SRIM	FLUKA	Expt.
^{238}U	3.722 ± 0.003	3.874 ± 0.007	3.442 ± 0.004	. . .
^{237}U	3.569 ± 0.003	3.713 ± 0.007	3.423 ± 0.007	3.456 ± 0.09

the xenon ion is in the region of uniform production rate) and an orange cross (where the kinetic energy of the xenon ion is in the range where FLUKA overestimates the production rate by the greatest extent). The location on the target marked by the green cross corresponds to the situation where xenon ions interact with the very first aluminum atoms on the surface of the target and successfully create ^{48}V fragments. In this situation, the created fragments gain the highest possible kinetic energy of 280 MeV/u (the initial energy of the xenon ions, 300 MeV/u, reduced by beam loss in the vacuum window and air). Residual activity of these fragments will be detected at the very end of the depth profile, since the range of the 280 MeV/u ^{48}V in aluminum amounts to 19.67 mm (labeled R_1 in Fig. 7). The location marked by the orange cross corresponds to the depth in the target at which the xenon ions reach an energy of 75 MeV/u, which is also the place where FLUKA makes its greatest overestimate of production of ^{48}V nuclides. The final depth of these fragments (labeled R_2 in Fig. 7) is equal to the sum of the penetration path of the xenon ions on which their kinetic energy is reduced from 280 MeV/u to 75 MeV/u and the range of ^{48}V with an energy of 75 MeV/u. From the stopping power calculations provided by ATIMA, it is possible to determine that the range $R_2 = 8.38 + 2.16 = 10.54$ mm. A closer look at the depth profile of the residual activity shows that the artificial peak (the orange area) of the residual activity is located at a depth of about 10.6 mm. This may be considered as a perfect match and explanation for the overestimation of the residual activity in the region downstream of the range, since FLUKA exaggerates the production of fragments in a range of few MeV/u.

The same approach may also be applied in the case of ^{46}Sc, ^{48}V, ^{52}Mn, ^{54}Mn, ^{56}Co, ^{58}Co, and ^{65}Zn nuclides, and therefore we can conclude beyond any doubt that the FLUKA code gives inaccurate results for residual activity in the case of intermediate-Z fragments.

From the depth profiling of the activity of the ^{237}U nuclide induced in target T_1, we observed that FLUKA predicts the presence of the nuclide in only two target foils, in contrast to the experimental results, where we observe it in three foils, although the geometry of the target was identical. This motivated us to use this technique for range verification of the primary beam and its fragments, as presented in Refs. 14, 16, and 18. In a similar fashion, we considered the range of the ^{237}U fragments, determined from the depth profiling to be equivalent to that of the ^{238}U ions, since the primary particles were not detectable in our experiment because of their long half-life. The range of the heavy-ion beams is approximately proportional to A/Z^2; therefore, the range of the ^{238}U should be longer than that of the ^{237}U by only about 0.4%, under the condition of matching initial energies. The measured and calculated ranges of both nuclides, together with the range straggling, are presented in Table II. ATIMA and SRIM overestimate the range of ^{238}U compared with the measured range of ^{237}U, and their relative deviations are 7.7% and 12.1%, respectively. At the same time, FLUKA predicts a shorter range of the primary projectiles, but the relative deviation is only 0.4%.

The range straggling of the ^{237}U and ^{238}U fragments calculated by SRIM and ATIMA is the same. On other hand, the FLUKA calculations give a range straggling of the ^{237}U fragments that is about two times larger than that of the ^{238}U primary projectiles. A logical explanation for this difference is that neither ATIMA nor SRIM implement inelastic interactions. Thus, they predict that the fragmentation occurs only on the surface of the target. In contrast, FLUKA simulates fragmentation processes at any depth of the target, which naturally influences both the range and the range straggling. In addition to this, SRIM and ATIMA consider a mono-energetic beam, whereas in the FLUKA calculations, beam parameters such as beam size and momentum spread are set

according to their experimental values, and this has an impact on range straggling, as has been shown in Ref. 16.

V. CONCLUSION

Depth profiling of the residual activity is an effective technique that provides an opportunity to benchmark different processes and physical phenomena within a single experiment. Activation of three aluminum targets by ^{238}U beams with energies 200 MeV/u and 125 MeV/u and a ^{124}Xe beam with energy 300 MeV/u were compared with simulated data provided by the FLUKA Monte Carlo code. Depth profiling of the residual activity of target-nuclei fragments in all the setups described in Table I revealed the same kind of discrepancies between experimental and calculated data. We demonstrated in the particular case of the T_1 target that the transition between nucleus–nucleus interaction models around an energy of 125 MeV/u is not correct. The shape of the simulated depth profile was not improved by changing the setting of the energy threshold between the relativistic quantum molecular dynamics (RQMD) and Boltzmann master equation (BME) models. Other misleading FLUKA calculations were found in the case of so-called intermediate-Z nuclides (with Z between 46 and 65 in our study) induced in the aluminum target T_3 by the 300 MeV/u ^{124}Xe beam. Through an additional set of simulations, we showed that the production rate of these fragments in thin foil by ^{124}Xe beams with different energies does indeed reach a maximum at a certain energy. An artificial peak in the depth profiles of these fragments could be explained as the sum of the depth at which the energy of the primary particles is reduced to the energy at the maximum production rate of the investigated fragment plus the range of fragments with this energy at the depth at which the primary ions are fragmented. The observations from all irradiations of aluminum targets reveal an overestimate in the prediction of residual activity upstream and/or downstream of the range region introduced by the nucleus–nucleus interaction models of FLUKA.

Attempted validation of the simulation code based on comparison of the inventory of identified nuclides in gamma spectra and those predicted by the simulations uncovered another imperfection in the code. Between 5 and 15 nuclides in a metastable state were found and identified in each of the experiments. Nevertheless, the simulations did not predict their production in the targets, since the FLUKA algorithm does not separate the radioactivity produced by nuclides in the isomeric state from that emitted by excited nuclides on their way to the ground state. We consider this number of nuclides rather significant (a few tens of nuclides per experiment), given the total number of the nuclides induced in the experimental targets after irradiation.

ACKNOWLEDGMENTS

This work has received support from HGS-Hire, as well as from BMBF (German Ministry for Research) during the time of this project.

REFERENCES

[1]L. Evans and P. Bryant, "LHC machine," J. Instrum. **3**, S08001 (2008).
[2]J. E. Leiss, "Impact of accelerators on United-States Science, technology, and productivity," IEEE Trans. Nucl. Sci. **30**(2), 1353–1356 (2017).
[3]X. S. Yan, L. Yang, X. C. Zhang, and W. L. Zhan, "Concept of an accelerator-driven advanced nuclear energy system," Energies **10**(7), 944 (2017).
[4]I. Hofmann, "Heavy ion accelerator-driven inertial fusion," Rev. Accel. Sci. Technol. **8**, 37–53 (2015).
[5]F. Winterberg, "On the ignition of small thermonuclear assemblies," Laser Part. Beams **36**, 232–235 (2018).
[6]A. C. Müller, "Nuclear waste incineration and accelerator aspects from the European PDS-XADS study," Nucl. Phys. A **751**, 453C–468C (2005).
[7]D. H. H. Hoffmann, A. Blazevic, P. Ni *et al.*, "Present and future perspectives for high energy density physics with intense heavy ion and laser beams," Laser Part. Beams **23**, 47–53 (2005).
[8]M. Kostin, G. Bollen, D. Georgobiani *et al.*, "Analysis of residual activity at the FRIB linear accelerator," J. Phys. Conf. Ser. **1046**, 012014 (2018).
[9]P. Spiller and G. Franchetti, "The FAIR accelerator project at GSI," Nucl. Instrum. Methods Phys. Res. A **561**, 305–309 (2006).
[10]J. C. Yang, J. W. Xia, G. Q. Xiao, H. S. Xu *et al.*, "High intensity heavy ion accelerator facility (HIAF) in China," Nucl. Instrum. Methods Part B **317**, 263–265 (2013).
[11]A. Fertman, E. Mustafin, R. Hinca, I. Strasik, M. Pavlovic *et al.*, "First results of an experimental study of the residual activity induced by high-energy uranium ions in steel and copper," Nucl. Instrum. Methods Phys. Res. B **260**, 579–591 (2007).
[12]A. A. Golubev, A. V. Kantsyrev, V. E. Luckjashin *et al.*, "Measurement of the energy deposition profile for U-238 ions with specific energy 500 and 950 MeV/u in stainless steel and copper targets," Nucl. Instrum. Methods Phys. Res. B **263**, 339–344 (2007).
[13]I. Strašík, E. Mustafin, and M. Pavlovič, "Residual activity induced by heavy ions and beam-loss criteria for heavy-ion accelerators," Phys. Rev. Spec. Top. - Accel. Beams **13**, 071004 (2010).
[14]V. Chetvertkova, I. Strašík, A. Belousov *et al.*, "Activation of aluminium by argon: Experimental study and simulations," Nucl. Instrum. Methods Phys. Res. B **269**, 1336–1340 (2011).
[15]E. Mustafin, T. Seidl, A. Plotnikov *et al.*, "Ion irradiation studies of construction materials for high-power accelerators," Radiat. Eff. Defects Solids **164**, 460–469 (2009).
[16]I. Strašík, V. Chetvertkova, E. Mustafin *et al.*, "Depth profiling of residual activity of ^{237}U fragments as a range verification technique for ^{238}U primary ion beam," Phys. Rev. Spec. Top. - Accel. Beams **15**, 071001-1–071001-13 (2012).
[17]I. Strašík, E. Mustafin, A. Fertman *et al.*, "Experimental study of the residual activity induced by 950 MeV/u uranium beam in stainless steel and copper," Nucl. Instrum. Methods Phys. Res. B **266**, 3443 (2008).
[18]P. Katrík, E. Mustafin, D. H. H. Hoffmann *et al.*, "Activation of accelerator constructing materials by heavy ions," Nucl. Instrum. Methods Phys. Res. B **365**, 525–528 (2015).
[19]G. Battistoni, F. Cerutti, A. Fasso *et al.*, "The FLUKA code: Description and benchmarking," AIP Conf. Proc. **896**, 31 (2007).
[20]A. Fasso, A. Ferrari, J. Ranft *et al.*, "FLUKA: A multi-particle transport code (program version 2011)," CERN-2005-10, INFT/TC_05/11, and SLAC-R-773T (2005).
[21]J. F. Ziegler, M. D. Ziegler, and J. P. Biersack, "SRIM—The stopping and range of ions in matter (2010)," Nucl. Instrum. Methods Phys. Res., Sect. B **268**, 1818 (2010).
[22]H. Weick, ATIMA (Energy loss of ions penetrating matter) (2016), available at http://www-linux.gsi.de/~weick/atima.html (November 1, 2016).
[23]K. Parodi, T. Bortfeld, W. Enghardt *et al.*, "PET imaging for treatment verification of ion therapy: Implementation and experience at GSI Darmstadt," Nucl. Instrum. Methods Phys. Res. A **591**, 282–286 (2008).
[24]H. Reeg and N. Schneider, "Current transformers for GSI's keV/u to GeV/u ion beams—An overview," in *Proceedings of DIPAC 2001* (ESRF, Grenoble, France, 2001), pp. 120–122.
[25]M. Schwickert, T. Hoffmann, F. Kurian *et al.*, "Diagnostic devices for beam intensity measurement at FAIR," in *Proceedings of IPAC2011* (JAcoW, San Sebastian, Spain, 2011), pp. 1174–1176.
[26]P. Forck, *Lectures Notes on Beam Instrumentation and Diagnostic* (Joint Universities Accelerator School, 2011).
[27]H. Reeg, "Performance Limitations of the DCCTs at GSI," in *Proceedings of Workshop on DC Current Transformers and Beam-Lifetime Evaluations* (CERN, Lyon, France, 2004), pp. 9–15.
[28]B. für Justiz, "Verordnung über den Schutz vor Schäden durch ionisierende Strahlen," (BGBl. I S. 2034, 2036) (2018), available at http://www.gesetze-im-internet.de/strlschv_2018/.